Transient Response of a Plate-Liquid System Under an Aerial Detonation : Simulation and Experiments

André Langlet, Mame William-Louis, Grégory Girault, Olivier Pennetier

Transient Response of a Plate-Liquid System Under an Aerial Detonation : Simulations and Experiments

André Langlet[a,*], Mame William-Louis[a], Grégory Girault[b], Olivier Pennetier[a]

[a] *Univ. Orleans, Ensi de Bourges, PRISME EA4229*
F45072, Orléans, France
[b] *Univ. Bretagne Sud, LIMATB, Rue Saint-Maudé, Centre de Recherche*
BP92116, 56321 Lorient, France

Abstract

This paper presents a mixed numerical approach to model the blast waves generated by the detonation of a spherical stoichiometric mixture of propane and oxygen, impacting a plate-liquid system. The problem is split into two parts. The first calculation part relies on the modeling of the blast load and its propagation. Over-pressure distribution, in this part, is presented and reveals a very good level of agreement with experimental results. The time and space scales of the blast load data must be compatible with the plate-liquid system. This compatibility is ensured by an appropriate spatio-temporal interpolation technique. This technique is presented and its effectiveness and accuracy are demonstrated. The second part consists in modeling the response of the coupled plate-liquid system under the numerical blast load model. Experiments at reduced scale are carried out in two configurations in order to assess the effectiveness of this mixed numerical approach. Convincing results are obtained and discussed.

Keywords: Blast wave, Plate-liquid system, Fluid-structure interaction, Cartesian methods, Reduced scale experiments

*corresponding author, 63 Av. de Lattre de Tassigny, F18020 Bourges Cedex, France
Email address: andre.langlet@univ-orleans.fr (André Langlet)

Notations

t	: Time	[s]
ρ_ℓ	: Fluid mass density	[kg.m^{-3}]
χ	: Fluid bulk modulus	[Pa^{-1}]
c_ℓ	: Speed of acoustic waves in the liquid	[m.s^{-1}]
ρ	: Plate mass density	[kg.m^{-3}]
E	: Plate Young modulus	[Pa]
ν	: Plate Poisson's ratio	
h	: Plate thickness	[m]
$I = h^3/12$	: Moment of inertia of the cross-section	[m^4]
$G = E/[2(1+\nu)]$	: Shear modulus	[Pa]
$D = EI/(1-\nu^2)$	: Flexural modulus	[Pa $\cdot$ m^4]
r_{plate}	: Maximum radius on the plate	[m]

1. Introduction

In this work we study the mechanical effect of an explosion in air over a flat plate resting on a quiescent fluid. The response of the plate - liquid system is determined by the fluid structure interaction which develops very rapidly owing to the blast wave of the explosion.

In practice, blast loads arise when solid or gas explosives detonate due to the ignition of high explosive materials. There is a real need to understand the effects of such loads on structures or on persons, for example, in the field of risk and industrial safety, risks prevention against terrorist attacks, or in military applications.

Conceptually, the explosion phenomenon can be broken down into the following phases: (i) the detonation process in the explosive medium, (ii) the shock propagation in the surrounding environment, (iii) the shock reflection by an obstacle wall, (iv) the response of the impacted structure and of the fluids and/or materials confined by the structure. These 4 phases correspond to 4 modeling steps involving multiphysical simulations: phase (i) is a reactive flow; phase (ii) deals with unsteady compressible fluid flow; phases (iii) and (iv) involve fluid structure interactions (FSI).

Blasts are created by underwater explosion (UNDEX) and in air explosions (INEX). The major difference between UNDEX and INEX is due to the dynamics of the gas core produced by the detonation of high explosives. In INEX the pressure of the gas core decreases (as the detonation products expand) until it reaches the atmospheric pressure. In UNDEX, the gas products form a bubble which experiences

alternate expanding-contracting motions. In UNDEX problems, the issue of cavitation is unavoidable; it has been studied by Geers & Hunter (2002), Sprague (2002), Galiev (1996), among others. Cavitation must be considered at the gas-liquid and at the fluid-structure interfaces. Experimental techniques dedicated to cavitation studies are presented by Herbert et al. (2006). The modeling of UNDEX and INEX must describe the differing nature of the phenomena due to the differing properties of the media in which the explosion takes place.

Explosions in air and their effects on structures have been widely investigated. A review concerning various aspects of the response of blast loaded plates was published by Rajendran & Lee (2009). There are two major approaches for investigating blast effects on structures.

Firstly, studies address the explosion phenomenon and its coupling with the structure. Numerical methods are elaborated to describe the shockwave ignition and propagation. For example, the equations of the reactive flow can be solved using the Eulerian multimaterial formulation with a finite element discretization (Alia & Souli, 2006). Thus, the interaction between the blast and the structure can be described within long durations after the beginning of the explosion (Zakrisson et al., 2011). However, these methodologies require a large amount of optimized numerical parameters as well as very long computational times. Consequently high frequency phenomena are difficult to capture accurately. Simplifications might be chosen, as done by Kambouchev et al. (2007) who applied the rigid-body assumption for the plate but, nevertheless, fully solved the FSI in a Lagrangian frame.

Secondly, only the mechanical response is sought without modeling the blast dynamics. Therefore, the loads are given as input functions such as decaying exponential, constant pulses, the parameters of which are tuned to match experimental data. Another kind of input data is the well-known US Army Technical Manual ConWep code providing empirical blast loading functions Neuberger et al. (2007), Longère et al. (2013). Here, the key point is to compute the response under such loads including finite transformations see for example Langdon et al. (2013). The simulations include user-defined materials (or "UMAT") Longère et al. (2013) programmed in commercial codes, mainly ABAQUS, LSDYNA, EUROPLEXUS. Different structures can be studied, ranging from a "simple" plate, Jacinto et al. (2001) and Neuberger et al. (2007), or a sandwich panel (Karagiozova et al., 2009) to very complex assembly such as a soldier helmet with composite and polymer materials (Grujicic et al., 2010) or laminated glass (Larcher et al., 2012).

The aforementioned commercial codes are indispensable tools for solving dynamics problems, especially with blasts and FSI, in complex real systems (such as vehicles, planes, ships, plants) for which a long time and global response is sought,

see for example studies on mine blast modeling (Grujicic et al. (2007)). However, as will be seen in this work, if very specialized aspects of the dynamic response are investigated, such as the *early response*, it might be more appropriate to develop fully controlled numerical codes which allow focusing the model on high frequency waves. In addition, fully controlled codes (or "white box") are better options than commercial codes for careful comparison with delicate and difficult experiments, as is the case in the present work.

The interaction of the impacted structure deformation with the blast must be taken into account if the solid wall experiences large displacements, which can interact significantly with the flow, (Børvik et al. (2009)). Such load durations may exist if explosions occur in confined zones and generate planar blast waves (e.g. tunnels, closed rooms). On the contrary, a wall exposed to an aerial explosion is loaded by a moving pressure front. In this case, the first movements of the target are small in amplitude, unable to modify the shock reflection; large displacements may occur when the loading is over.

The exlposive used in the present work creates a source-explosion. Therefore, the incident waves are spherical, and the wave reflections are due mainly to oblique incident waves. According to the studies by Baker et al. (1973), Kinney (1962), the mechanism of this reflection can be accurately described. When the wave reaches the plate, the incident angle is zero. Kinney has shown that if this angle is lower than a certain limit, the reflection is regular. Beyond this limit the reflected wave cannot maintain the flow parallel to the wall. Then, it follows that the incident and the reflected waves coalesce in a triple point, and form a third shock wave which is detached from the wall — the Mach reflection. This shock is stronger and faster than the incident shock. The distance between the triple point and the wall increases as the reflection phenomenon goes on. For spherical shock waves, the locus of the triple point forms a curve away from the wall. The reflection of a shock wave on a structure is a complex phenomenon. Reflection coefficients are influenced by the shock characteristics and the properties of the atmosphere in which the reflection takes place Wadley et al. (2010).

From the point of view of structural dynamics, the considered blast pressure is a moving load, from its onset to its end. When the blast sweeps a wall, the rise time of the pressure is very short (a few μs for small scale detonations associated with over-pressure about 10^5 Pa) and occurs over a very narrow distance. This is why the moving pressure front is usually approximated by a discontinuity in analytical studies. The front starts to move with supersonic velocities (relatively to the acoustic wave in the fluid or in the structure) which rapidly decrease to subsonic velocities.

The first particularity of the present work is that the transient response of the

plate is calculated only during the time the blast wave impacts the plate. Structural waves are analyzed before any reflection occurs at the boundaries. The second particularity is that the response is strongly influenced by the coupling with the underlying fluid. Indeed, in such very short times the fluid reacts on the structure due to its compressibility, and also with an added mass effect. In the two media, the small perturbations theory may be applied, namely, elastic waves and acoustic waves form the present response observed without boundary influences. Researching early time responses may rely on some hypotheses. For example, Sprague & Geers (1999) applied partial series closure for solving the response of a spherical shell under a spherical shock. Here, the early response is separated into a closed-form portion (representing a planar wave approximation for the fluid-shell interaction), and a complementary mode-sum portion. Unlike such an approach, we have made a direct simulation, which benefited from some specific features of the fast dynamic response, as it will appear in section 6. While cavitation is an unavoidable issue in UNDEX, it is a remaining question to determine wheter cavitation occurs behind the plate considered in this study. In fact the pure acoustic fluid model may lead to negative pressure which may be less than the hydrostatic pressure; this suggests going further in the modeling. However, in the present work, we have focused the analysis on the very early stages of the system response observed in laboratory experiments with reduced scale explosions. The understanding of the coupled plate response and the modeling both rely on previous works we have done on analytical stationary responses of the plate system(Renard et al. (2003), Renard & Langlet (2008)), with an acoustic model for the fluid. This is why cavitation was not considered in the paper. When comparing experiments with simulations, care was taken to verify that the numerical fluid pressure never fell below the hydrostatic pressure with moderate explosions. In the experiments, the explosive energy was limited to that used in the modeling. In the time considered the response takes the form of waves undisturbed by the boundaries. This is why real complex fluid – structure systems may be simplified since only elements of them are set into movement. This is an additional argument for designing in-house numerical codes rather than engaging full direct modeling with heavy commercial codes.

In the present work, the numerical simulation deals with both the explosion and the response of a plate-liquid system. Experimental results with reduced scale detonations have confirmed the results of this simulation. The explosion is supposed to occur at a given height over the plate resting on the liquid. Phases (i), (ii) and (iii) are solved numerically by direct simulations (CFD modeling) of the chemical energy release during the detonation, and of the propagation of the shock wave in the atmosphere above the plate. Phase (iv) is solved by an explicit scheme based on

the finite differences (FD) approximation for the equations of motion for the plate and the fluid. The blast pressure load is applied to the plate-liquid model as the computations proceed, so that the load faithfully reproduces the pressure variations of the external flow field. The objective is to capture the high frequency components of the waves with acceptable accuracy and reliability. One assumption is that the acoustic coupling with the atmosphere ahead of the load front is disregarded: only the coupling with the fluid supporting the plate is modeled.

The choice of this particular experimental configuration, consisting of an aerial explosion over a plate, is motivated by the useful results it provides, both for the modeling approach and for the engineers.

2. Numerical model for the blast load

The dynamic and thermal behaviors of the propagation phenomena of a blast wave are governed by the unsteady transport equations for mass, momentum and energy. Viscous and thermal diffusion processes may play a significant role in the overall transport phenomena, but they are not included in the conventional diffusion terms leading to the Navier - Stokes equations, as this would require very fine spatial discretization in the regions with strong velocity and temperature gradients. The corresponding grid scales would be extremely small and, thus, would involve mesh sizes beyond the capacity of the computers currently available. Consequently, the effects of viscous and thermal diffusion are implemented as global source terms added to the transport equations. This unsteady Euler three-dimensional problem is solved by a software developed in-house. The numerical method involves an unstructured finite-volume cell-centered approach that couples the classic second-order upwind scheme with the two-step Van Leer time-explicit integration scheme. This coupling yields a second-order accurate-in-space-and-time method. In order to prevent the numerical oscillations that can occur in regions with strong gradients, the classical minmod limiter is used. Initially, the flow is assumed to be at rest throughout the three-dimensional domain, except inside the sphere (of radius r_b) that contains the explosive charge. In this sphere, the flow is disturbed by the blast wave calculated by the use of a one-dimensional spherical procedure that is made compatible with the three-dimensional mesh thanks to the 1D - 3D remapping algorithm. In this zone, the hot detonation gases obey the Jones - Wilkins - Lee (JWL) law. Details of this mixed method, combining 1D and 3D cartesian methods, are described in Benselama et al. (2009).

As an illustration, a blast wave impacting a rigid wall is depicted in Fig. 1 for different times. This figure shows the incident wave arriving at time $t_A(0)$ as well as

the reflected one. It also shows the Mach stem (MS) appearing as well as the triple point (T).

3. Numerical model of the plate-liquid system

3.1. The coupled system

The physical system is represented in Fig. 2. The liquid in contact with the plate is assumed to be inviscid and compressible. Its compressibility must be taken into account since it is submitted to fast loading. The velocity of the sound waves in the fluid is: $c_\ell = \sqrt{1/(\rho_\ell \chi)}$. The fluid governing equations are derived under the small perturbations hypothesis. The Helmoltz equations can be derived by combining (i) the constitutive equation of the fluid, (ii) the equation of motion, (iii) the mass conservation equation, and by using the velocity potential φ:

$$\frac{\partial^2 \varphi}{\partial t^2} = c_\ell^2 \Delta \, \varphi \tag{1}$$

The fluid pressure (denoted by p_i) is:

$$p_i = \rho_\ell \frac{\partial \varphi}{\partial t} \tag{2}$$

The equations of motion for the plate may be classically derived from the Hamilton's principle with appropriate formulations of the virtual works of respectively: internal forces (tensile and compressive forces, bending moments, shearing forces), and of the external loads. The Mindlin Reissner's assumption Mindlin (1951) is retained for the plate dynamics, which includes shear deformations. Also, the angular cross-section rotation, ψ (Fig. 2) is associated with its proper inertia. This improvement of the plate theory is necessary for small wavelengths, Mindlin (1951). Under this assumption, Girault (2006) wrote an appropriate formulation in order to take into account the nonlinear effects of the membrane stresses in the plate, which may arise for high amplitude loads.
Since the blast load is axisymmetric, the response of the plate needs to be sought too. Therefore the equations of motion are expressed in cylindrical coordinates, (r, θ, respectively the radial and polar coordinates) retaining only the radial distance r for the spatial dependence. Then, in a polar coordinate system, for an axisymmetric plate and under the Mindlin-Reissner hypothesis, three components are necessary to describe the displacement of particles belonging to the plate middle-surface: radial

displacement u, out of plane displacement w, and rotation ψ of the normal vectors to the undeformed middle surface in the $(r,\,\theta)$ plane. The axisymmetric plate with thickness h is submitted to the external load p_e and to the fluid pressure p_i. Thus, the motion of a particle belonging to the plate neutral surface is modeled by:

$$\begin{aligned} r\rho\, h\frac{\partial^2 u}{\partial t^2} &= \frac{\partial(rN_{rr})}{\partial r} - N_{\theta\theta} \\ \frac{1}{12}r\rho\, h^3\frac{\partial^2 \psi}{\partial t^2} &= \frac{\partial(rM_{rr})}{\partial r} - M_{\theta\theta} + rQ \\ r\rho\, h\frac{\partial^2 w}{\partial t^2} &= \frac{\partial(rQ)}{\partial r} + \left[rN_{rr}\frac{\partial w}{\partial r}\right] - p_e\, r + p_i\, r \end{aligned} \tag{3}$$

where (per unit length): N_{rr}, $N_{\theta\theta}$, are respectively the radial and hoop membrane forces, M_{rr}, $M_{\theta\theta}$ stand for the radial and hoop moments and Q designates the shear force. These forces and moments are obtained by integration of the stress components over the plate cross section.
It has been shown by Girault (2006) that the combination of the fluid added mass effect with the fluid elastic response considerably enhances the stiffness of the plate-liquid system. Therefore, the coupling with the fluid does not allow the onset of nonlinear effects during the loading by the blast wave. So, only the linear terms of the plate equations are retained in the present study. Neglecting terms for membrane stresses N_{rr}, $N_{\theta\theta}$, the previous equations are expressed using the displacement components:

$$\begin{aligned} M_{rr} &= D\left(\frac{\partial \psi}{\partial r} + \nu\frac{\psi}{r}\right) \\ M_{\theta\theta} &= D\left(\frac{\psi}{r} + \nu\frac{\partial \psi}{\partial r}\right) \\ Q &= \kappa G h\left(\frac{\partial w}{\partial r} - \psi\right) \end{aligned} \tag{4}$$

It results in the following second order partial differential equations:

$$\begin{aligned} \rho\, I\frac{\partial^2 \psi}{\partial t^2} &= D\left(\frac{\partial^2 \psi}{\partial r^2} + \frac{1}{r}\frac{\partial \psi}{\partial r} - \frac{\psi}{r^2}\right) + \kappa\, G h\left(\frac{\partial w}{\partial r} - \psi\right) \\ \rho\, h\frac{\partial^2 w}{\partial t^2} &= \kappa\, G h\left(\frac{\partial^2 w}{\partial r^2} - \frac{\partial \psi}{\partial r} + \frac{1}{r}\frac{\partial w}{\partial r} - \frac{\psi}{r}\right) - p_e + p_i \end{aligned} \tag{5}$$

A shear factor $\kappa = 5/6$ is introduced, which is related to a non constant shear stress distribution over the cross section. For the present plate theory the two characteristic velocities are c_s and c_p – the velocity of longitudinal waves and of shear waves, respectively:

$$c_p = \sqrt{\frac{E}{\rho(1-\nu^2)}} \tag{6}$$

$$c_s = \sqrt{\frac{\kappa\, G}{\rho}} \tag{7}$$

The coupling conditions between the plate and the liquid are ensured by the continuity of normal forces and displacements at the interface. Therefore, the following condition must be verified at any time:

$$\frac{\partial w}{\partial t} = -\frac{\partial \varphi}{\partial z}\bigg|_{z=0} \tag{8}$$

Introducing the radius of gyration $r_0 = h/\sqrt{12}$ as the characteristic length, and $t_0 = r_0/c_p$ as the characteristic time, all variables and functions are made non-dimensional. Non dimensional terms will be written in capital letters. Note that $\psi = \Psi$ at homologous points. Three non-dimensional ratios are sufficient to parameterize the coupling between the plate and the liquid:

$$\theta = \frac{c_s}{c_p} \tag{9}$$

$$\delta = \frac{c_\ell}{c_p} \tag{10}$$

$$\mu = \frac{\rho_\ell}{\rho\sqrt{12}} \tag{11}$$

Then, the unknown functions are $W = W(R,T)$, $\Psi = \Psi(R,T)$ and $\Phi = \Phi(R,Z,T)$. The axisymmetric problem to be solved can be expressed in the following non-dimensional form:

$$\frac{\partial^2 \Psi}{\partial T^2} = \frac{\partial^2 \Psi}{\partial R^2} + \frac{1}{R}\frac{\partial \Psi}{\partial R} - \frac{\Psi}{R^2} + \theta^2 \left(\frac{\partial W}{\partial R} - \Psi\right) \tag{12}$$

$$\frac{\partial^2 W}{\partial T^2} = \theta^2 \left(\frac{\partial^2 W}{\partial R^2} + \frac{1}{R}\frac{\partial W}{\partial R} - \frac{\partial \Psi}{\partial R} - \frac{\Psi}{R} \right) + \mu \left. \frac{\partial \Phi}{\partial T} \right|_{Z=0} - P_e \tag{13}$$

$$\frac{\partial^2 \Phi}{\partial T^2} = \delta^2 \left(\frac{\partial^2 \Phi}{\partial R^2} + \frac{1}{R}\frac{\partial \Phi}{\partial R} + \frac{\partial^2 \Phi}{\partial Z^2} \right) \tag{14}$$

$$\frac{\partial W}{\partial T} = - \left. \frac{\partial \Phi}{\partial Z} \right|_{Z=0} \tag{15}$$

Eqs. (12) and (13) are the equations of motion for the plate loaded by the blast pressure P_e and the fluid pressure P_i. Eq. (14) is the equation of the fluid motion which takes the form of an acoustic wave equation. The coupling condition ensuring the continuity of the normal velocity components at the plate-fluid interface is expressed by Eq. (15). The symmetry and interface conditions are detailed in Appendix A.

3.2. An adapted explicit finite difference scheme.

The plate equations, the coupling conditions at the interface with the underlying liquid, are discretized over a uniform grid (with space increments ΔR and ΔZ). The first and second order derivatives of the coupled system and of the coupling conditions (Appendix A) are approximated by finite difference (FD) at each node and time. The time integration can be performed using the numerical schemes of the Newmark family. These schemes depend explicitly on two parameters whose values allow to modify the nature of the integration scheme, from pure implicit to pure explicit integration formulae. For dynamics problems, explicit integration is preferred in order to capture the fast events of the coupling. Some refinements can be adopted in order to control or to reduce spurious oscillations due to spatial discretization. In a context of explicit time integration, one can refer to classical dissipative schemes developed by Newmark (1959), Chung & Lee (1994), Zhai (1996), Hulbert & Chung (1996). Maheo et al. (2011) discusse and compare the performances of these dissipative schemes for academic problem of 1D and 3D impacted bar.
For fluid–structure interaction, one has to choose between partitioned and monolithic schemes. The partitioned scheme allows to solve the equations for fluid and solid separately according to a staggered procedure (Park et al., 2010). Contrariwise, the monolithic scheme allows to simultaneously solve flow and structural equations so that their mutual influence can be taken into account directly, which is favorable for the stability of the calculation (Breuer et al., 2012)
In this study, classical centered finite difference formulae are used to approximate the first and second order derivatives. A pure explicit time integration is adopted, and

a monolithic approach is retained at the interface between the plate and the fluid, at $Z = 0$. Let $X^k = {}^t\{\Psi, W, \Phi\}$ be the unknown vector at the current time step, $T^k = k\Delta T$. After replacing the partial derivatives with their corresponding finite difference operators, and rearranging the equations, the following algebraic system is obtained:
(i) At the interface ($Z = 0$):

$$X^{k+1} = [\mathbf{A}]\, X^k + [\mathbf{B}]\, X^{k-1} + [\mathbf{C}]\, R_i^k \tag{16}$$

(ii) In the fluid domain ($Z < 0$):

$$\Phi^{k+1} = 2\Phi^k - \Phi^{k-1} + R_\ell^k \tag{17}$$

where:

$$[\mathbf{A}] = \frac{2}{1+\alpha\,\beta} \begin{bmatrix} 1+\alpha\,\beta & 0 & 0 \\ 0 & 1 & \alpha \\ 0 & -\beta & 1 \end{bmatrix} \tag{18}$$

$$[\mathbf{B}] = \frac{-1}{1+\alpha\,\beta} \begin{bmatrix} 1+\alpha\,\beta & 0 & 0 \\ 0 & 1-\alpha\,\beta & 2\alpha \\ 0 & -2\beta & 1-\alpha\,\beta \end{bmatrix} \tag{19}$$

$$[\mathbf{C}] = \frac{\Delta T^2}{1+\alpha\,\beta} \begin{bmatrix} 1+\alpha\,\beta & 0 & 0 \\ 0 & 1 & \alpha \\ 0 & -\beta & 1 \end{bmatrix} \tag{20}$$

In these equations, terms $\alpha = \mu\Delta T/2$ and $\beta = -\delta^2\Delta T/\Delta Z$ depend on the mesh and time discretizations. Terms R_i^k stand for the FD formulation of the right hand side of Eqs. (13), (12), (14) at the interface for the current time step while R_ℓ^k denotes the FD formulation of the right-hand side of Eq. (14) in the fluid domain. Formulation of R_i^k and R_ℓ^k varies according to the coupling and symmetry conditions, as recalled in Appendix A.
In order to ensure the stability of the numerical scheme, the time step ΔT must be lower than the minimum of the CFL condition established for the plate alone or for the fluid alone, according to Renard et al. (2003). In addition, the space increments must not exceed $1/10^{th}$ of the smallest wave length that is to be captured. For a given load front velocity $V = v/c_p$, the wave lengths deduced from the stationary analysis by Renard & Langlet (2008) are used as references.

4. Formulation of the blast pressure load on the plate by interpolation.

Following the impact of the blast wave (Fig. 1), the pressure spreads over the plate. This pressure load, computed by the CFD code, proceeds with specific time and space scales. The plate and liquid domains use different time and space discretizations to solve the explicit scheme previously described. Therefore, a special technique must be used in order to evaluate the correct pressure at a definite location and time over the plate domain. This pressure evaluation is based on a linear interpolation of the CFD pressure which must faithfully verify the time and space dependent nature of the blast wave. This method makes possible to compute the plate-liquid system response in parallel with the CFD computation of the blast wave. The principle of the procedure is illustrated in Fig. 3.
Let n be the nodes defined by the CFD model; $n = 0, \cdots, N$. It is assumed that the reflected pressure is known at every node n behind the shock front position. The pressure is zero ahead of the front position. The question is how to determine the pressure at nodes j required by the numerical scheme which calculates the response of the coupled plate. The arrival time $t_A(n)$ at node n is defined according to the following criterion. When the pressure $p(n,t)$ begins to rise, the time t^* and pressure p^* for which the maximum rate of rise $dp(n,t)/dt$ occurs are detected; then $t_A(n)$ is the time where the line of equation:

$$\left[\frac{dp(n,t)}{dt}\right]_{max} \times (t - t^*) + p^* \tag{21}$$

intersects the time axis.
As nodes n may not coincide with nodes j of the plate, an interpolation is applied to evaluate the pressure at nodes j. The pressure at abscissa r_j is determined from the pressure histories at nodes n and $n+1$, such that: $r_n \leq r_j \leq r_{n+1}$. As Δr_n is small, the velocity of the pressure front may be considered as constant in the duration $\Delta t_A = t_A(n+1) - t_A(n)$. Between nodes n and $n+1$ the velocity of the front is approximated by:

$$v = \frac{\Delta r_n}{\Delta t_A} \tag{22}$$

Hence, the arrival time at node j is given by:

$$t_A(j) = t_A(n) + \frac{r_j - r_n}{v} \tag{23}$$

As the pressure depends on r and t, the interpolation must use appropriate times in order to take into account the time shifts between pressure histories, respectively at nodes n, j, $n+1$:

$$\Delta t_A(n) = t_A(j) - t_A(n) \tag{24}$$

$$\Delta t_A(n+1) = t_A(n+1) - t_A(j) \tag{25}$$

It is assumed that these time shifts remain constant for all times.
At radial abscissa r_j and time t, the pressure is interpolated as follows :

$$t_n = t - \Delta t_A(n) \qquad p_n = p(r_n, t_n) \tag{26}$$

$$t_{n+1} = t + \Delta t_A(n+1) \qquad p_{n+1} = p(r_{n+1}, t_{n+1}) \tag{27}$$

$$\begin{aligned} p(r_j, t) =& \frac{p_{n+1} - p_n}{t_{n+1} - t_n} (t - t_n) + p_n \\ p(r_j, t) =& \frac{\Delta t_A(n)}{\Delta t_A(n) + \Delta t_A(n+1)} (p_{n+1} - p_n) + p_n \end{aligned} \tag{28}$$

When two nodes j and n coincide, the interpolation procedure has been shown to perfectly return the given pressure p_n. For example, using data for experimental case 35-223, Fig. 4 illustrates the results of an interpolation in the vicinity of $r = 0.2$ m.

5. Experimental methods

In this work, an experimental system has been designed to investigate gaseous detonations and their effects on structures, (Girault, 2006). This system makes it possible to carry out multi-scale studies on the response of experimental models. In the present case, the explosion occurs over a flat plate located under the explosion plane. A stoichiometric mixture of propane and oxygen ($C_3H_8 + 5O_2$) is used as the explosive. For a temperature of 20 °C, the values of the mass density and of the specific energy are, respectively: 1.414×10^{-3} g/cm^3 and 14.16 MJ/m^3.
The gas is confined in a hemispherical “soap" bubble formed on the bench. The required confinement is obtained by injecting the gaseous mixture in an aqueous solution of sodium oleate. An electrical ignition system is used to create the gas detonation. Firstly, capacitors (8 μF) are charged under 7500 V. Secondly, the rapid discharge of these capacitors induces an energy flow which is sufficient to vaporize a thin copper wire (10^{-1} mm diameter), welded between two tungsten electrodes located in the center of the reactive gas. The “exploded wire" provides enough energy (approximately 55 J) to make the gaseous mixture detonate. A spherical

shock wave is then generated inside the confinement, which leads to a blast wave at the interface between the reactive medium and the air. The energy of the detonation is evaluated from the specific energy of the gaseous mixture. It is assumed that the exploded wire energy is entirely consumed in the ignition.
In configuration 1, Fig. 5, a 80 cm square plate lying underneath a second flat plate placed at a distance d_n ("normal distance") is considered. The upper plate is equipped with the ignition device and gas supplying tubes. The gas is confined in hemispherical soap bubbles formed on the upper wall, and centered on the ignition device. When the gas is injected in the soap water mixture, a liquid film is forms. It inflates until its radius reaches the radius of a circular template, which ensures the expected explosive mass. The lower plate is equipped with three pressure sensors, labeled B, C, and D. Sensor B is just under the explosion center. Sensors C and D are located 187 mm and 254 mm away from B, respectively.
In configuration 2 (Fig. 6), the explosive gas is confined in a soft balloon because the sizes of the required confinements are not easy to maintain when using the soap bubble technique. Configuration 2 is used for gas confinements larger than 100 mm diameters. The radiuses of the balloons are controlled by a metallic circle. The ignition and supply devices are placed at the balloon center. The square aluminum plates which were tested were also 80 cm in width, and were maintained in contact with the water filling an 80 cm deep-tank. Sensor A – which is placed at the same stand-off distance d_n from the plate and the explosion center – measures a reference pressure. This sensor is hit by the shock wave arriving at point O ($r = 0$). Its signal gives the same over-pressure as that which would be measured at point O. Because of the various reflections on the flat plate, only the beginning of the pressure history A can be compared to the reflected pressure at point O.
Table 1 sums up the experimental configurations considered in this study.

6. Numerical Simulations and Comparison with test results

6.1. Pressure validation

The reproducibility of the pressure histories has been extensively studied, using configuration 1. Pressure measurements were made on a surrogate rigid plate fitted with Kistler 603B sensors placed at three radial locations: B, C, D, on the two lines 1 (polar angle $\theta = 0$ degree, Fig. 5) and 2 (polar angle 45 degree). Measurements at C and D for the two lines nearly overlap each other, which clearly proves the symmetry of the pressure distribution.
Numerical simulation results are presented for the experimental case 35-223, configuration 1.This enables a validation of the reflected pressure over the lower wall.

Comparison of the numerical pressures for case 35-223 with experimental pressure records at locations B, C, and D, are plotted in Fig. 7. Here, only measurements obtained on line 2 are plotted, since records on line 1 are equivalent. The calculated pressure and the measured pressure are very close to each other, as shown in Fig. 7. The rise time, the over pressure and the exponential decay, are clearly well predicted.

6.2. Transient response of the plate liquid - system.

The parameters used in the simulation are valid for cases 60-220, 62.5-283. The material properties of the plate and of the liquid are given in Table 2 and Table 3. In Figures 8, 9, and 10, one can observe the propagation and reflection of pressure fields at selected times, both in the fluid domain and over the plate. The chronology of the events is linked to the speeds at which the waves propagate. The speed is constant in the fluid (c_ℓ). On the contrary, the continuously decreasing speed of the load front generates waves of various frequencies whose speeds are determined by the dispersion function of the coupled plate-liquid system. At first glance, Fig. 8, 9, and 10, indicate that some of the plate movements propagate ahead of the Mach stem location. The calculated pressure in the fluid cannot be less than -10^5 Pa in relative value.
The diagram showing the evolution in space and time of the flexural strains

$$\varepsilon_{rr} = -\frac{h}{2}\frac{\partial \psi}{\partial r} \tag{29}$$

is helpful to understand the phenomenon before any reflection on the boundaries. Due to the small thickness of the plate ($h = 0.5$ mm) in case 62.5-283, Fig. 11, the frequencies contained in the response are much higher than in case 60-220 ($h = 5$ mm), Fig. 12. The explanation is that for the non-dimensionnal solution of system (12), (13), (14), and (15), the length scale is $h/\sqrt{12}$ and the time scale is $h\sqrt{\rho(1-\nu^2)/(12E)}$. Therefore, in thin plates, solutions will exhibit smaller wave lengths than in thick plates composed of the same material. This is justification for defining the thickness h as the characteristic length, as it was pointed out earlier, (see, for example, Miklowitz (1980)). In Fig. 11, the shock front is marked by the dotted line. The slope of this line in the $r-t$ plane represents the velocity of the load front. It can be seen that this slope decreases rapidly, and then remains close to an almost constant value. Oscillations emerge and spread ahead from the load front. Although the stationary conditions are not absolutely fulfilled, the frequencies and wavelengths of these oscillations are not far from those forecast by the stationary analysis presented in Renard et al. (2003) and Renard & Langlet (2008). Indeed, in

a short distance and time interval, the speed of the load and its amplitude do not vary significantly. Then, considering the high values of the shock wave speed, large numbers of oscillations appear in this short duration. Over the thicker plate the front velocity stabilizes at approximately $v = 426$ m/s during the time intervals considered in this work. For this case, an analytical calculation based on the methodology presented in Renard & Langlet (2008) forecasts a wavelength of 0.08 m. The comparison with the present numerical result is very satisfactory since the wavelength of the oscillations is close to 0.07 m. It should be noted that a perfect matching of the wavelengths is not possible because: (i) the plate is of finite dimension; (ii) the actual propagation is cylindrical and the mechanical response contains a transient part; an exact stationary response is valid only for an infinite system submitted to a uniform moving load. In the present paper, the spatial and time increments (ΔR, ΔZ, ΔT) of the numerical scheme have been chosen so that, for large system sizes, a uniform pressure P_0 moving at constant speed v gives a response consistent with analytical results in Renard & Langlet (2008) – for v comprised in intervals of the system characteristic velocities. Ideally, this uniform load moving at constant speed is expressed with the Heaviside function in the coordinate system used:

$$P_e = P_0 \mathrm{H}(VT - R) \tag{30}$$

where H is the Heaviside function.
Numerically, the jump of the pressure depends upon the discretization parameters. The influences exerted by these parameters were analyzed using the Heaviside load (30) over the sets of nodes n, as the given load curves prior to the pressure interpolation in the calculation procedure. This has permitted supplementary investigations about the validity of the rise time of the CFD pressure. In order to assess how the response is affected by the sampling of the CFD pressure, the detonation pressure has been replaced by a uniform pressure traveling with a constant speed. The rise time can thus be parameterized. Two calculations (plate thickness 5 mm) have been made, using the pressure 10^5 Pa, traveling with the velocity 1334.4 m/s (or $V = 0.25$), and rise time of 15 μs and 3 μs, respectively. The 3 μs rise time, is in the order of the value observed in the experiments, while 15 μs is the average of the numerical rise time of the CFD model. With parameters such as the ones used here, the theoretical wavelength of the stationary response harmonic component (according to Renard & Langlet (2008)) is $\lambda = 2.304$ cm. The wave length obtained with the present model is $\lambda = 2.380$ cm. Fig. 13 shows that the consistency between the two results is remarkable if the response to the Heaviside load (30) and to the blast load are plotted together against the relative coordinate $r - r^*$, (r^* is the shock front instantaneous

coordinate).
To sum up at this point, spatial and time steps were validated if they led to results that were consistent with analytical solutions. The influences exerted by the rise time of the pressure load curves on lowering the frequency contents of the response were found to be acceptable.
To compare the simulations and the experiments, Fig. 14 and Fig. 15, presents the results for case 60-220, while Fig. 16, and Fig. 17 presents those for case 62.5-283. In addition, the arrival times $t_A(0)$ and the load front velocity vs. r are plotted in Fig. 18 and Fig. 19.
For the propane - oxygen explosive gas, experimental results given in Brossard et al. Brossard et al. (1995) provide the arrival time and the load front velocity, which are plotted in solid line the radial coordinate r in Fig. 18 and Fig. 19, respectively; these plots correspond to the experimental data of case 60-220. According to Fig. 18, the mean difference between the ordinates of the two curves is about 22 μs. This order of magnitude concerning the arrival time has been found in the three simulation cases associated with the three experimental cases (35-223, 60-220, 62.5-283). This is why the simulated results of strains have been shifted in time by 22 μs.
The velocity curve obtained from Brossard et al. (1995) (Fig. 19) is considered as a reference because it has been established with a large number of experiments, and with the same gaseous explosive as in our experiments. This curve is compared to the same function deduced from the present CFD computations (cross symbols) for the case 60-220. Obviously, the two curves are very close, except for small r values, that stand for short times following the impact of the shock on the plate. In fact, near the origin O, the theoretical speed for a spherical shock reflecting on a flat plate is infinite. According to Fig. 19, the velocity of the load deduced from Brossard et al. (1995) and of the CFD pressure are close to each other when the velocities decrease slowly along the r coordinate. Therefore, it could be expected at first, that the frequencies components of the response will be similar whether the present pressure results or the one in Brossard et al. (1995) are used. Since the rise time of the pressure front in the CFD model is lower than that of Brossard et al. (1995), clearly, contributions of high frequency components of the response will be underestimated. This is why the amplitudes and the apparent period are lower than the ones observed in the experimental records, especially if the experimental signals reveal high frequencies in the response (Fig. 17).

7. Conclusion

The following results are to be highlighted:

- The unsteady flow equations for air blasts were solved with a home house CFD code.
- The simulation of the plate–liquid system under this blast load has been validated.
- Space and time scales of the CFD and structural models are made compatible.
- Experimental strains and pressures show good agreement with the simulations.

Concerning the blast load, comparisons with experimental results reveal that the simulations captured the specific features of the pressure histories (the over pressure, positive and negative phase durations, impulse). Furthermore, analysis of the structural system demonstrates that the rise time of the pressure has been simulated with a good accuracy, which allows us to compute the high frequency components of the response up to a good level of accuracy.
The transient response of the system was computed only in times for which the blast pressure travels over the plate. In these durations (typically less than 1 ms), it is shown that the theoretical stationary analysis presented in previous works is relevant. Indeed, due to the high velocities of the loads generated by an explosion, the movements are very fast and they develop undisturbed by the boundary conditions in small space and time intervals, as if the domain were infinite. Based on the stationnary results, the analysis has shown that the inherent limitation of the numerical method does not affects the relevance of the results. When it comes to longer times, however, a complete tridimensional modeling would be necessary if physical coupling was to be investigated, which is beyond the scope of the present study.
In the experimental study, the explosions were obtained by the detonation of a propane-oxygen gaseous mixture. Analyzing the ability of CFD codes to predict transient responses is justifiable only if the experimental pressure fields are sufficiently similar to those created by solid explosives defined with appropriate energy equivalence.
In conclusion, this work has provided a basis for studying more complex coupling between the blast and the structure-liquid system. It provides improved numerical tools which can be used with more complex deformable structures, but do not require the use of predetermined pressure load curves, as the latter may lead to inaccurate predictions.

Acknowledgements

The authors are grateful to Professor Philippe Gillard for providing hardware facilities which were needed for the present work.

Appendix A. Coupling and symmetry conditions.

If $R = 0$, the symmetry implies:

$$\left.\frac{\partial W}{\partial R}\right|_{R=0} = \left.\frac{\partial \Phi}{\partial R}\right|_{R=0} = 0, \qquad \Psi = 0 \tag{A.1}$$

If $R \to 0$, de l'Hôpital's rule leads to:

$$\lim_{R\to 0} \frac{\Psi}{R} = \left.\frac{\partial \Psi}{\partial R}\right|_{R=0} \tag{A.2}$$

$$\lim_{R\to 0} \frac{1}{R}\frac{\partial \Psi}{\partial R} = \left.\frac{\partial^2 \Psi}{\partial R^2}\right|_{R=0} \tag{A.3}$$

If $Z = 0$, a second order Taylor expansion of function Φ on variable R leads to:

$$\left.\frac{\partial^2 \Phi}{\partial Z^2}\right|_{Z=0} = \frac{2}{\Delta Z^2}\left[\Phi(\Delta Z) - \Phi(0) - \left.\frac{\partial \Phi}{\partial Z}\right|_{R=0} \Delta Z\right]$$

Replacing $-\partial\Phi/\partial Z$ by $\partial W/\partial T$:

$$\left.\frac{\partial^2 \Phi}{\partial Z^2}\right|_{Z=0} = \frac{2}{\Delta Z^2}\left[\Phi(\Delta Z) - \Phi(0) + \frac{\partial W}{\partial T}\Delta Z\right] \tag{A.4}$$

Time derivatives are grouped on the left-hand side, and the spatial derivative on the right-hand side.

$\underline{R = 0, \quad Z = 0}$:

$$\Psi(0, T) = 0 \tag{A.5}$$

$$\frac{\partial^2 W}{\partial T^2} - \mu \left.\frac{\partial \Phi}{\partial T}\right|_{Z=0} = 2\theta^2 \left[\frac{\partial^2 W}{\partial R^2} - \frac{\partial \Psi}{\partial R}\right] - P_e(R, T) \tag{A.6}$$

$$\frac{\partial^2 \Phi}{\partial T^2} - \frac{2\delta^2}{\Delta Z}\frac{\partial W}{\partial T} = 2\delta^2 \left\{\frac{\partial^2 \Phi}{\partial R^2} + \frac{1}{\Delta Z^2}\left[\Phi(\Delta Z) - \Phi(0)\right]\right\} \tag{A.7}$$

$\underline{R > 0, \quad Z = 0:}$

$$\frac{\partial^2 \Psi}{\partial T^2} = \frac{\partial^2 \Psi}{\partial R^2} + \frac{1}{R}\frac{\partial \Psi}{\partial R} - \frac{\Psi}{R^2} + \theta^2 \left[\frac{\partial W}{\partial R} - \Psi\right] \tag{A.8}$$

$$\frac{\partial^2 W}{\partial T^2} - \mu \frac{\partial \Phi}{\partial T}\bigg|_{Z=0} = \theta^2 \left[\frac{\partial^2 W}{\partial R^2} + \frac{1}{R}\frac{\partial W}{\partial R} - \frac{\partial \Psi}{\partial R} - \frac{\Psi}{R}\right] - P_e(R,T) \tag{A.9}$$

$$\frac{\partial^2 \Phi}{\partial T^2} - \frac{2\delta^2}{\Delta Z}\frac{\partial W}{\partial T} = \delta^2 \left\{\frac{\partial^2 \Phi}{\partial R^2} + \frac{1}{R}\frac{\partial \Phi}{\partial R} + \frac{2}{\Delta Z^2}\left[\Phi(\Delta Z) - \Phi(0)\right]\right\} \tag{A.10}$$

$\underline{R = 0, Z < 0:}$

$$\frac{\partial^2 \Phi}{\partial T^2} = \delta^2 \left[2\frac{\partial^2 \Phi}{\partial R^2} + \frac{\partial^2 \Phi}{\partial Z^2}\right] \tag{A.11}$$

$\underline{R > 0, Z < 0:}$

$$\frac{\partial^2 \Phi}{\partial T^2} = \delta^2 \left[\frac{\partial^2 \Phi}{\partial R^2} + \frac{1}{R}\frac{\partial \Phi}{\partial R} + \frac{\partial^2 \Phi}{\partial Z^2}\right] \tag{A.12}$$

References

Alia, A., & Souli, M. (2006). High explosive simulation using multi-material formulations. *Applied Thermal Engineering*, *26*, 1032 – 1042.

Baker, W. E., Dodge, S. T., & Westine, P. S. (1973). *Similarity Methods in engineering dynamics*. Hayden Book Company.

Benselama, A. M., William-Louis, M. J.-P., & Monnoyer, F. (2009). A 1d–3d mixed method for the numerical simulation of blast waves in confined geometries. *Journal of Computational Physics*, *228*, 6796 – 6810.

Børvik, T., Hanssen, A., Langseth, M., & Olovsson, L. (2009). Response of structures to planar blast loads – a finite element engineering approach. *Computers & Structures*, *87*, 507 – 520.

Breuer, M., Nayer, G. D., Munsch, M., Gallinger, T., & Wuchner, R. (2012). Fluid-structure interaction using a partitioned semi-implicit predictor-corrector coupling scheme for the application of large-eddy simulation. *Journal of Fluids and Structures*, *29*, 107 – 130.

Brossard, J., Desrosier, C., Purnomo, H., & Renard, J. (1995). A new family of explicit time integration methods for linear and non–linear structural dynamics. *Shock Waves @ Marseille*, *IV*, 387–392.

Chung, J., & Lee, J. (1994). A new family of explicit time integration methods for linear and non–linear structural dynamics. *Int. J. Numer. Method Eng.*, *37*, 3961–3976.

Galiev, S. (1996). Experimental observations and discussion of counterintuitive behavior of plates and shallow shells subjected to blast loading. *International Journal of Impact Engineering*, *18*, 783 – 802.

Geers, T. L., & Hunter, K. S. (2002). An integrated wave-effect model for an underwater explosion bubble. *J. Acout. Soc. Am*, *111*, 1584 – 1601.

Girault, G. (2006). *Réponse d'une plaque couplée à un liquide et soumise à une pression mobile. Aspects théoriques et expérimentaux en détonique*. Ph.D. thesis PhD Dissertation, Univ. Orléans, France.

Grujicic, M., Bell, W., Pandurangan, B., & He, T. (2010). Blast-wave impact-mitigation capability of polyurea when used as helmet suspension-pad material. *Materials & Design*, *31*, 4050 – 4065.

Grujicic, M., Haque, I., Roy, W. N., & Skaggs, R. R. (2007). Computational analysis of mine blast on a commercial vehicle structure. *Multidiscipline Modeling in Mat. and Str.*, *3*, 431 – 460.

Herbert, E., Balibar, S., & Caupin, F. (2006). Cavitation pressure in water. *Phys. Rev. E.*, *74*.

Hulbert, G. M., & Chung, J. (1996). Explicit time integration algorithms for structural dynamics with optimal numerical dissipation. *Computer Methods in Applied Mechanics and Engineering*, *137*, 175 – 188.

Jacinto, A. C., Ambrosini, R. D., & Danesi, R. F. (2001). Experimental and computational analysis of plates under air blast loading. *International Journal of Impact Engineering*, *25*, 927 – 947.

Kambouchev, N., Noels, L., & Radovitzky, R. (2007). Numerical simulation of the fluid-structure interaction between air blast waves and free–standing plates. *Computers & Structures*, *85*, 923 – 931.

Karagiozova, D., Nurick, G., & Langdon, G. (2009). Behaviour of sandwich panels subject to intense air blasts – part 2: Numerical simulation. *Composite Structures*, *91*, 442 – 450.

Kinney, G. (1962). *Explosive Shocks in Air*. Mac Millan, London.

Langdon, G., Karagiozova, D., von Klemperer, C., Nurick, G., Ozinsky, A., & Pickering, E. (2013). The air-blast response of sandwich panels with composite face sheets and polymer foam cores: Experiments and predictions. *International Journal of Impact Engineering*, *54*, 64 – 82.

Larcher, M., Solomos, G., Casadei, F., & Gebbeken, N. (2012). Experimental and numerical investigations of laminated glass subjected to blast loading. *International Journal of Impact Engineering*, *39*, 42 – 50.

Longère, P., Geffroy-Grèze, A.-G., Leblé, B., & Dragon, A. (2013). Ship structure steel plate failure under near-field air – blast loading: Numerical simulations vs experiment. *International Journal of Impact Engineering*, *62*, 88 – 98.

Maheo, L., Grolleau, V., & Rio, G. (2011). On the use of some numerical damping methods of spurious oscillations in the case of elastic wave propagation. *Mechanics Research Communications*, *38*, 81 – 88.

Miklowitz, J. (1980). *The theory of elastic waves and waveguides*. North Holland Publishing Company.

Mindlin, R. (1951). Influence of rotatory inertia and shear on flexural motions of isotropic plates. *Journals of Applied Mechanics*, *18*, 31–38.

Neuberger, A., Peles, S., & Rittel, D. (2007). Scaling the response of circular plates subjected to large and close-range spherical explosions. part i: Air-blast loading. *International Journal of Impact Engineering*, *34*, 859 – 873.

Newmark, N. (1959). A method of computation for structural dynamics. *J. Eng. Mech. Div. ASCE*, (pp. 67–94).

Park, K., Ohayon, R., Felippa, C., & González, J. (2010). Partitioned formulation of internal and gravity waves interacting with flexible structures. *Computer Methods in Applied Mechanics and Engineering*, *199*, 723 – 733.

Rajendran, R., & Lee, J. (2009). Blast loaded plates. *Marine Structures*, *22*, 99 – 127.

Renard, J., & Langlet, A. (2008). Moving pressure running over a plate coupled with a liquid: The analytical stationary response in the one–dimensional case. *Journal of Sound and Vibration*, *310*, 650 – 662.

Renard, J., Langlet, A., & Pennetier, O. (2003). Response of a large plate-liquid system to a moving pressure step. transient and stationary aspects. *Journal of Sound and Vibration*, *265*, 699 – 724.

Sprague, M. (2002). *Advanced Computational Techniques for the Analysis of 3-D Fluid-Structure Interaction with Cavitation*. Ph.D. thesis PhD Dissertation Univ. of Colorado at Boulder.

Sprague, M., & Geers, T. (1999). Response of empty and fluid-filled, submerged spherical shells to plane or spherical, step-exponential waves. *Schock and Vibration*, *6*, 147 – 157.

Wadley, H., Dharmasena, K., He, M., McMeeking, R., Evans, A., Bui-Thanh, T., & Radovitzky, R. (2010). An active concept for limiting injuries caused by air blasts. *International Journal of Impact Engineering*, *37*, 317 – 323.

Zakrisson, B., Wikman, B., & Häggblad, H.-A. (2011). Numerical simulations of blast loads and structural deformation from near-field explosions in air. *International Journal of Impact Engineering*, *38*, 597 – 612.

Zhai, W. (1996). A new family of explicit time integration methods for linear and non–linear structural dynamics. *Int. J. Numer. Method Eng.*, *39*, 4199–4214.

Tables

Configuration	1	2	2
Case number	35-223	60-220	62.5-283
Radius of explosive	35 mm	60 mm	62.5 mm
Distance d_n	223 mm	220 mm	283 mm
Plate material	Wood	Aluminum	Aluminum
Plate thickness	40 mm	5 mm	0.5 mm
Pressure sensors	B-C-D	A	A
strain gage locations	None	200 - 300 mm	200 - 300 mm

Table 1: Data for the experimental configurations.

	θ	c_p	E	ν	ρ
Plate	0.55	5337 ms^{-1}	7.2×10^{10} Pa	0.3	2790 $\mathrm{kg\,m}^{-3}$

Table 2: Plate material parameters.

	δ	μ	c_ℓ	ρ_ℓ
Liquid	0.28	0.1	1500 $\mathrm{m\,s}^{-1}$	$10^3 \mathrm{kg\,m}^{-3}$

Table 3: Liquid material parameters.

Figures

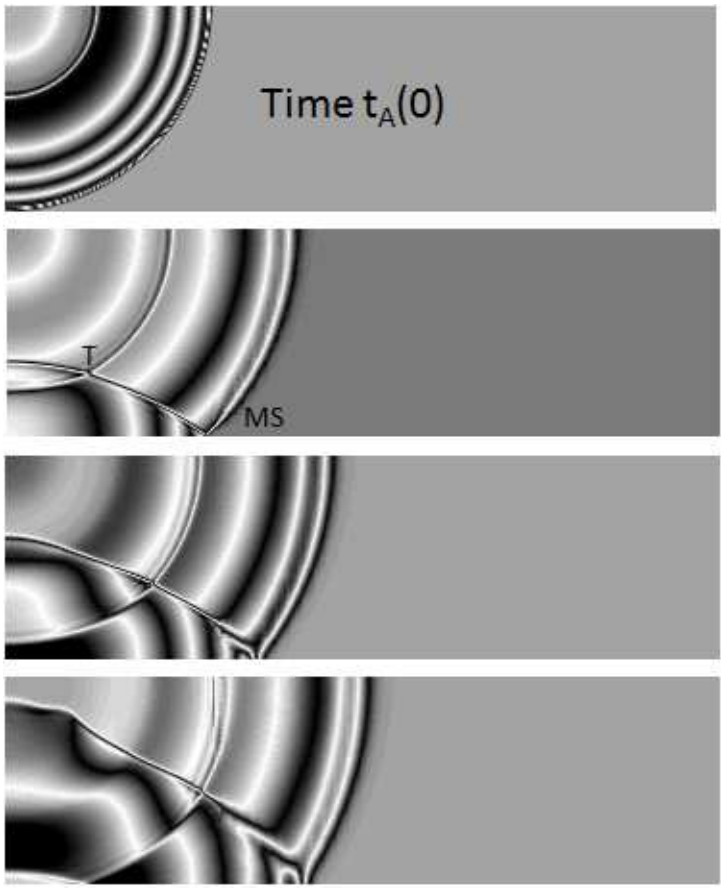

Figure 1: Propagation and reflection of the blast wave. Isomach levels. Case 60-220.

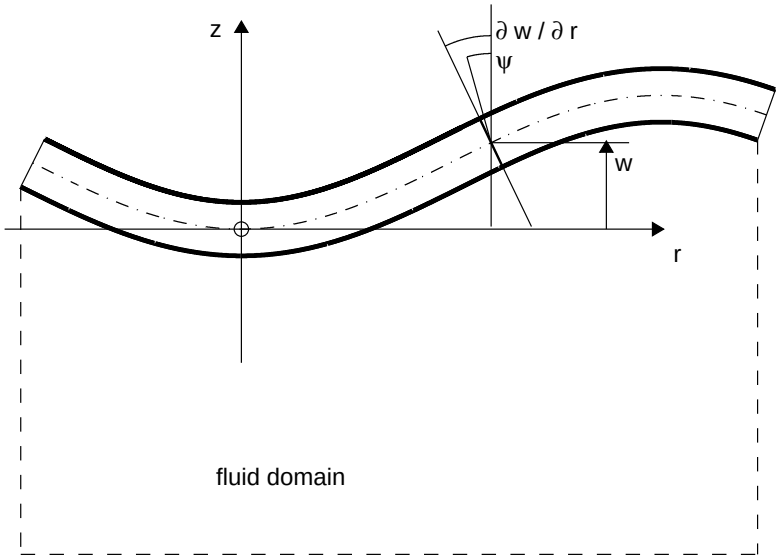

Figure 2: The plate-liquid system.

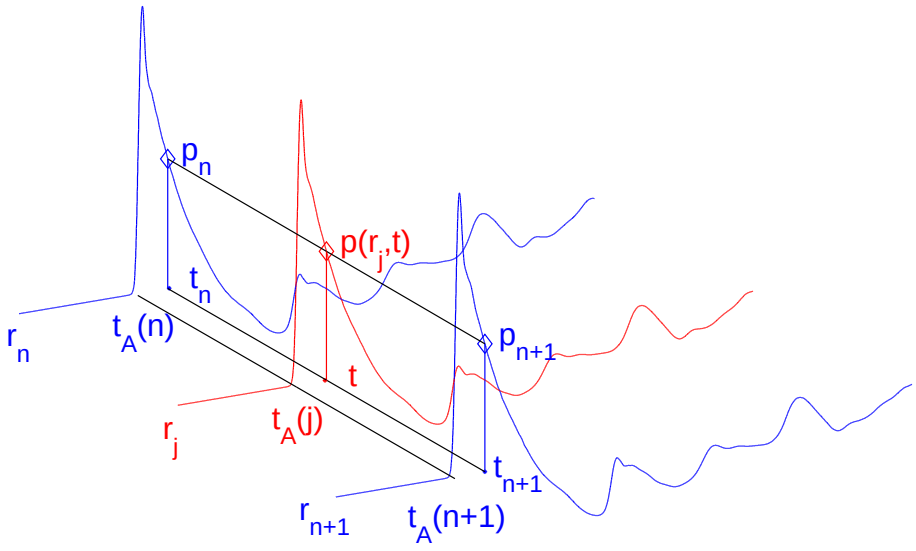

Figure 3: The interpolation method.

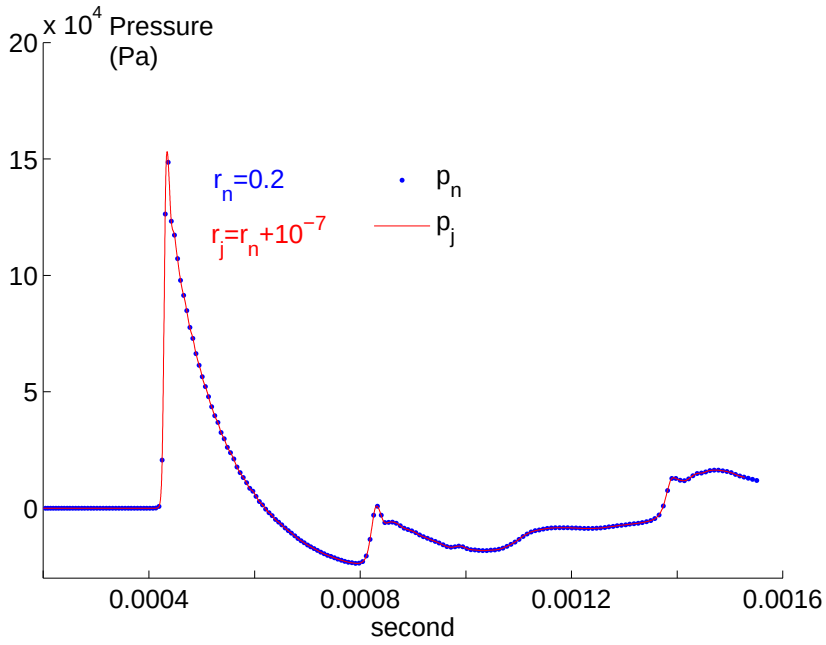

Figure 4: Verification of the interpolated pressure results.

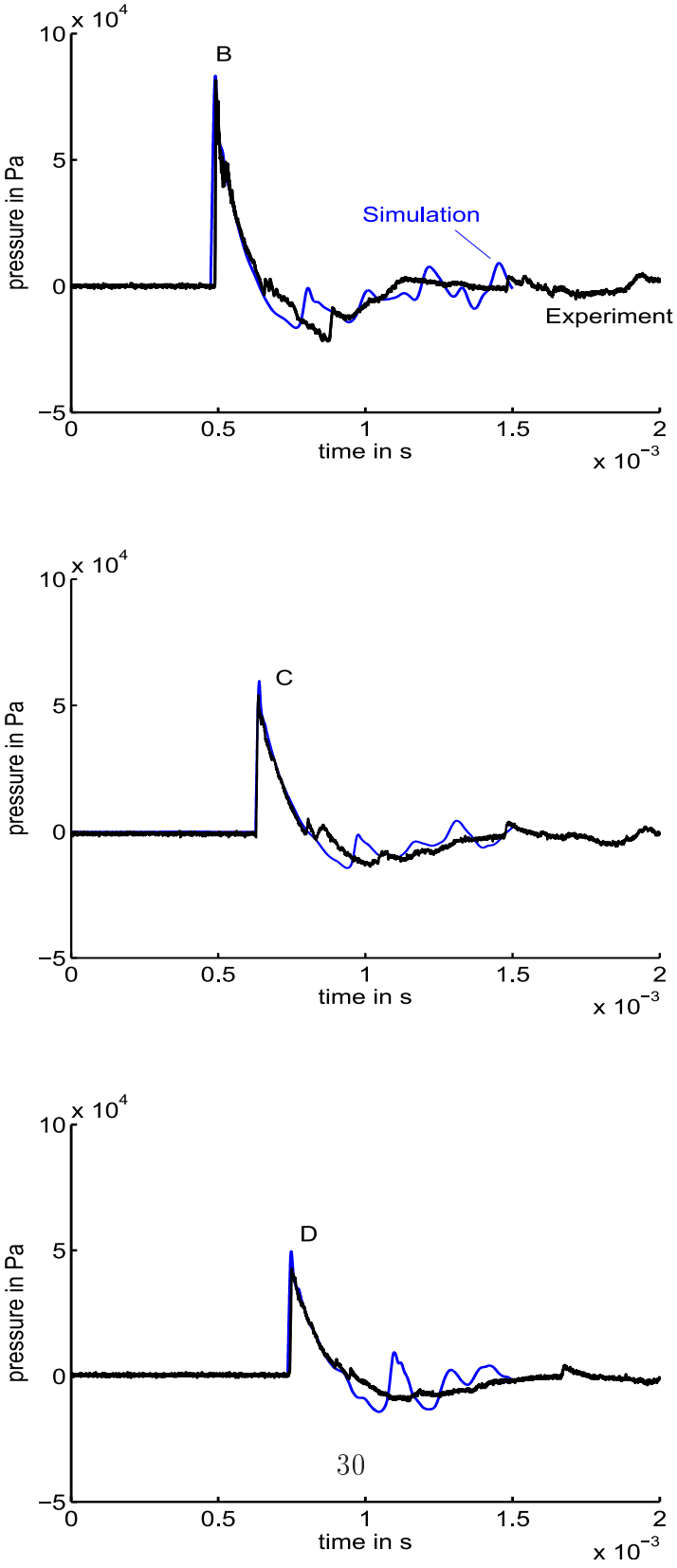

Figure 7: Comparison of computed and measured pressures in configuration 1.

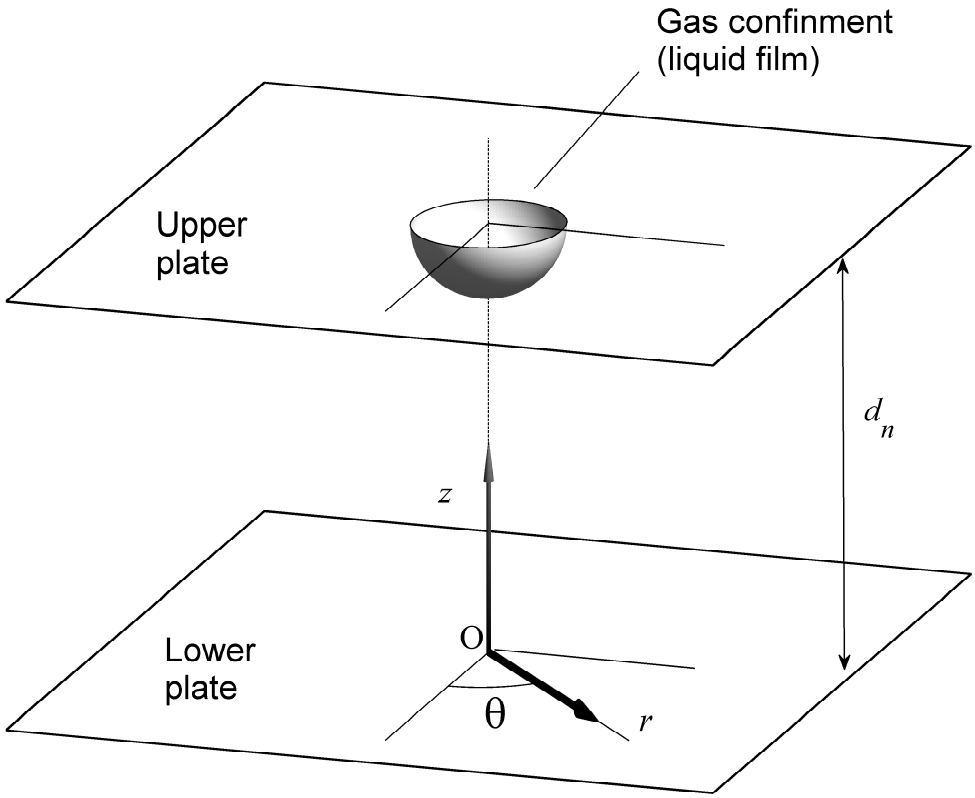

Figure 5: Experimental set-up for configuration 1.

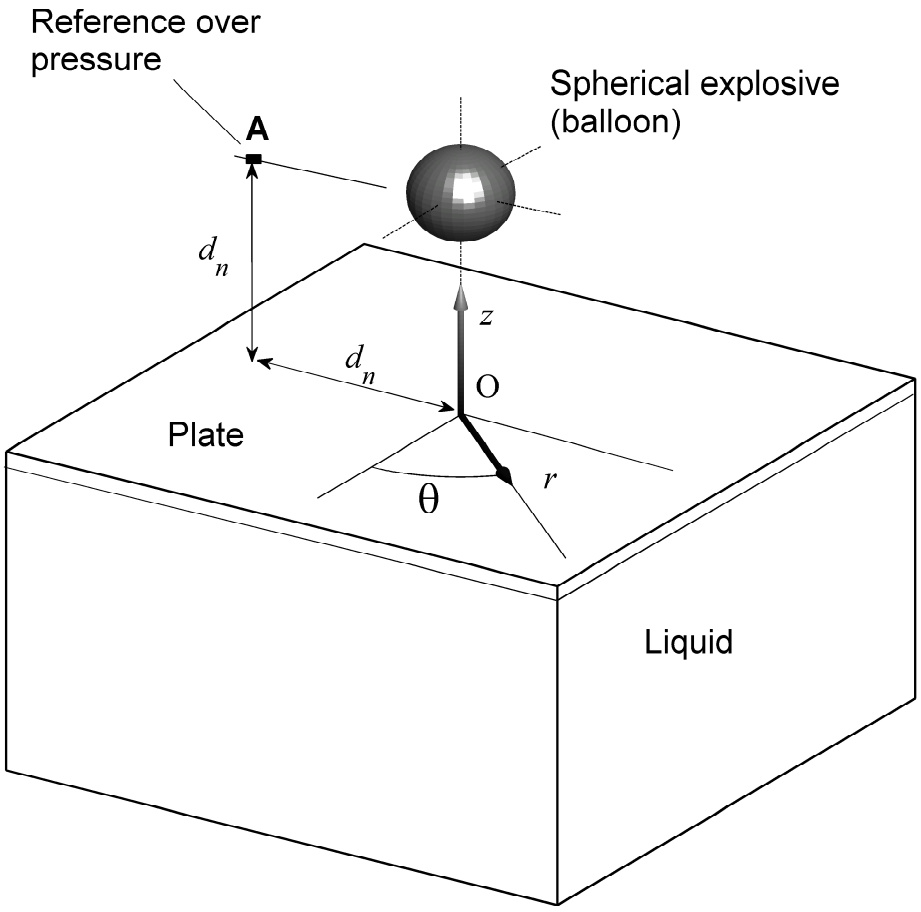

Figure 6: Experimental set-up for configuration 2.

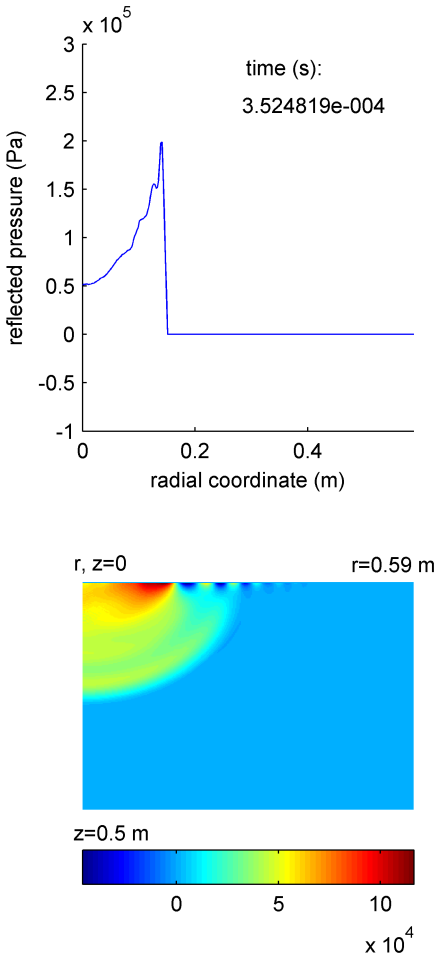

Figure 8: Pressure load and pressure (Pa) in the fluid at time 352 microseconds. Case 60-223.

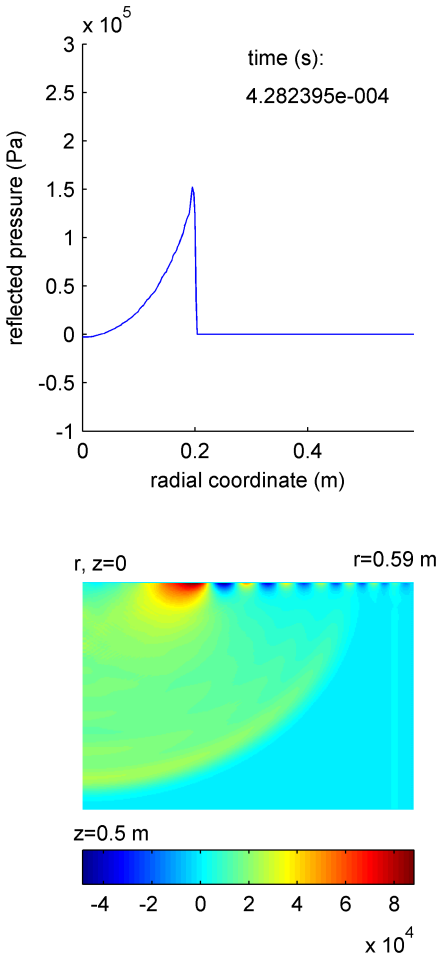

Figure 9: Pressure load and pressure (Pa) in the fluid at time 428 microseconds. Case 60-220.

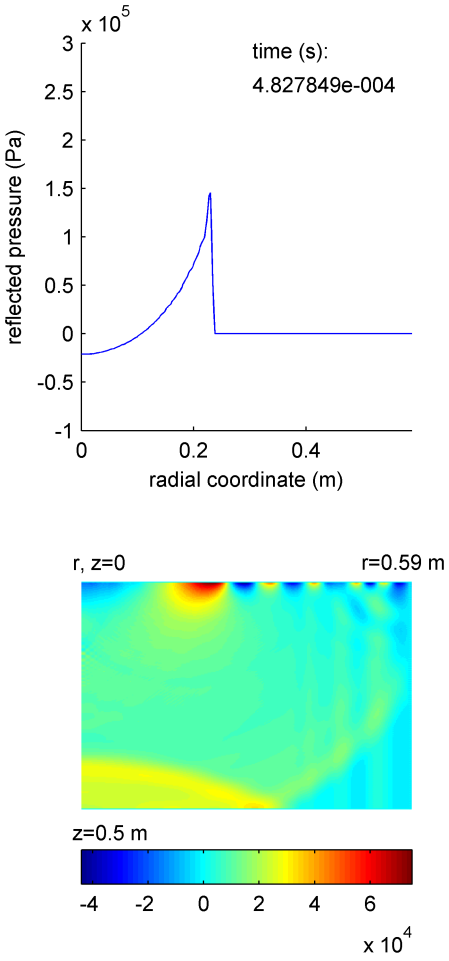

Figure 10: Pressure load and pressure (Pa) in the fluid at time 483 microseconds. Case 60-220.

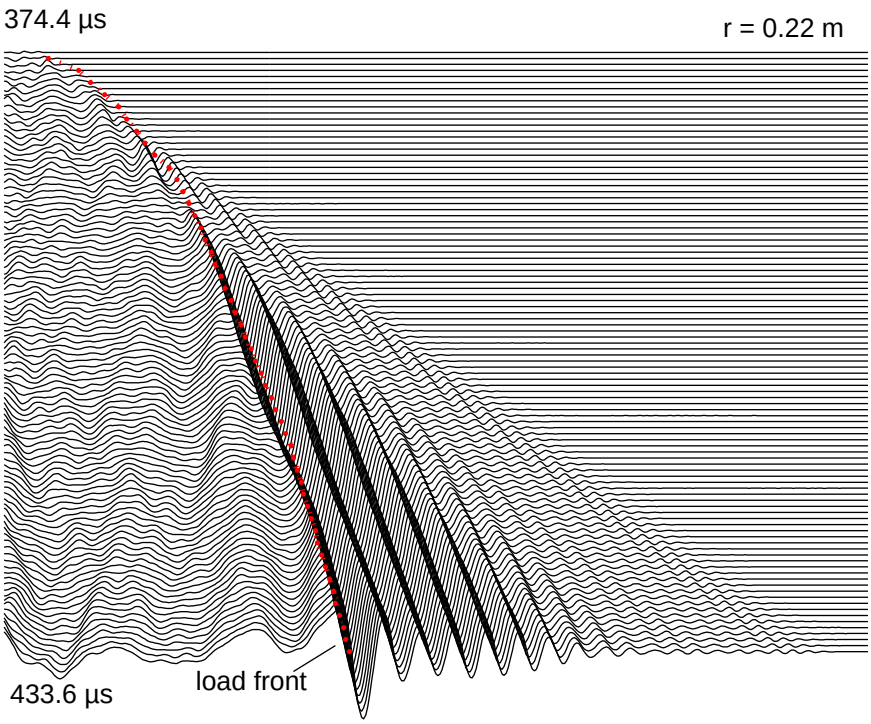

Figure 11: Evolution of the strains ε_{rr} in case 62.5-283.

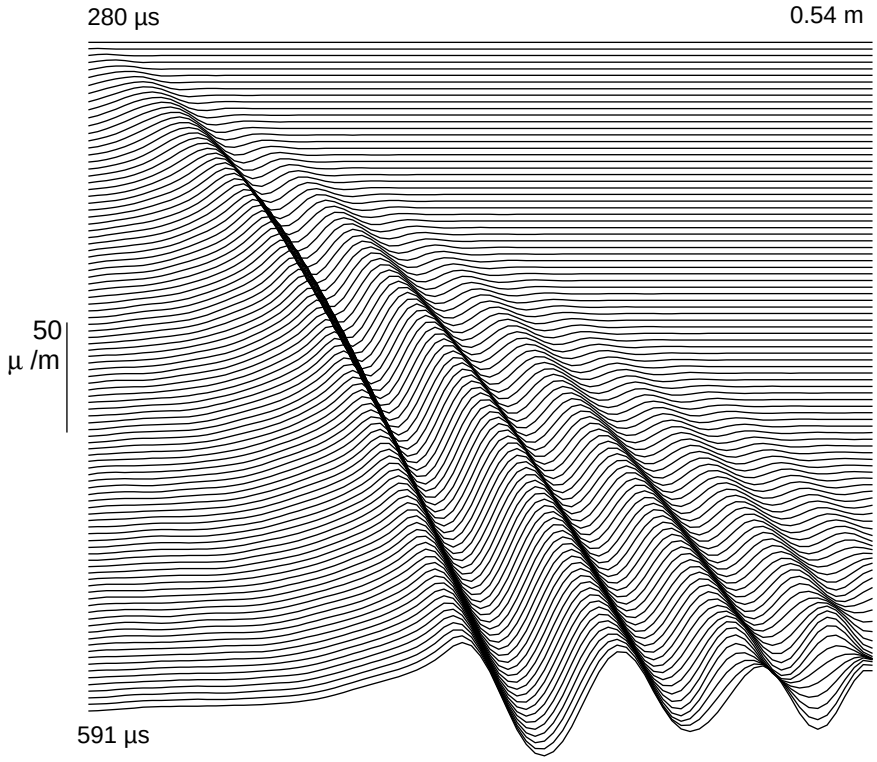

Figure 12: Evolution of the strains ε_{rr} in case 60-220.

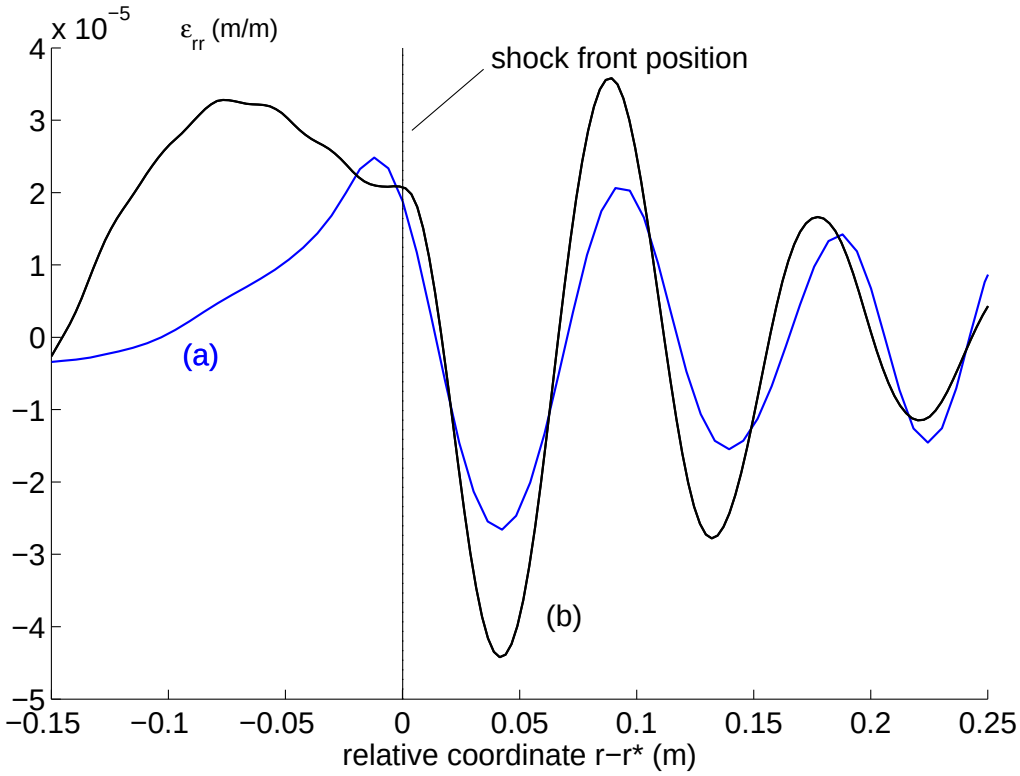

Figure 13: Flexural strains computed with the blast pressure (a) case 60-220, and (b) with the constant pressure moving at 426 m/s.

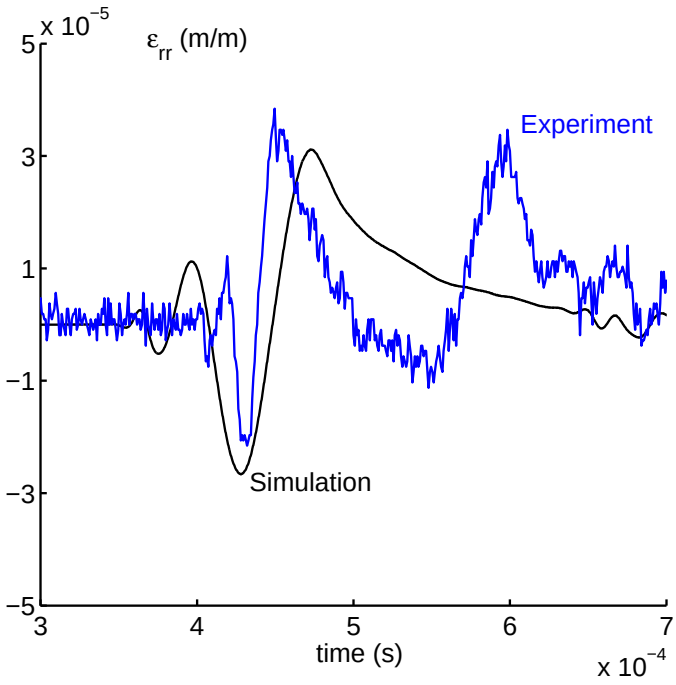

Figure 14: Simulation and experimental results for configuration 2, 60-220, at $r = 200$ mm.

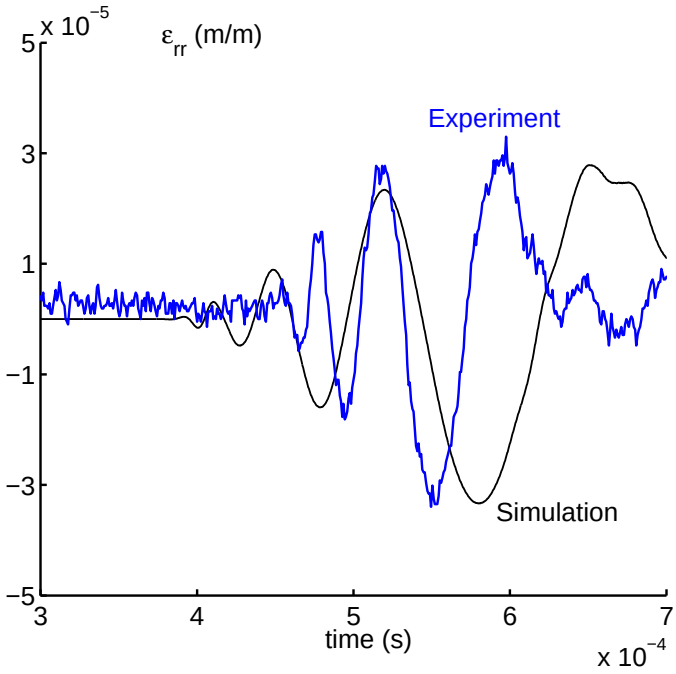

Figure 15: Simulation and experimental results for configuration 2, 60-220, at $r = 300$ mm.

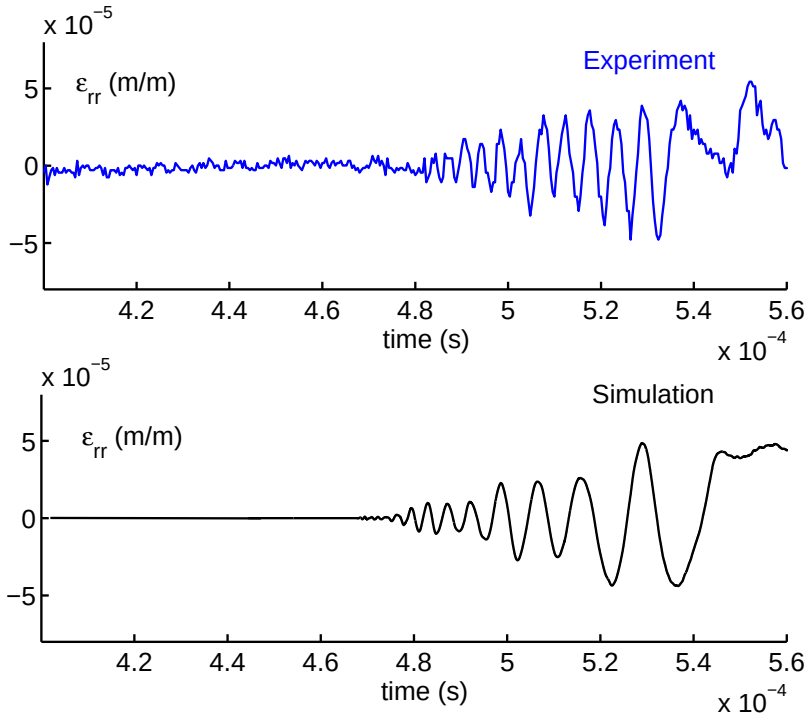

Figure 16: Simulation and experimental results for configuration 2, 62.5-283, at $r = 200$ mm.

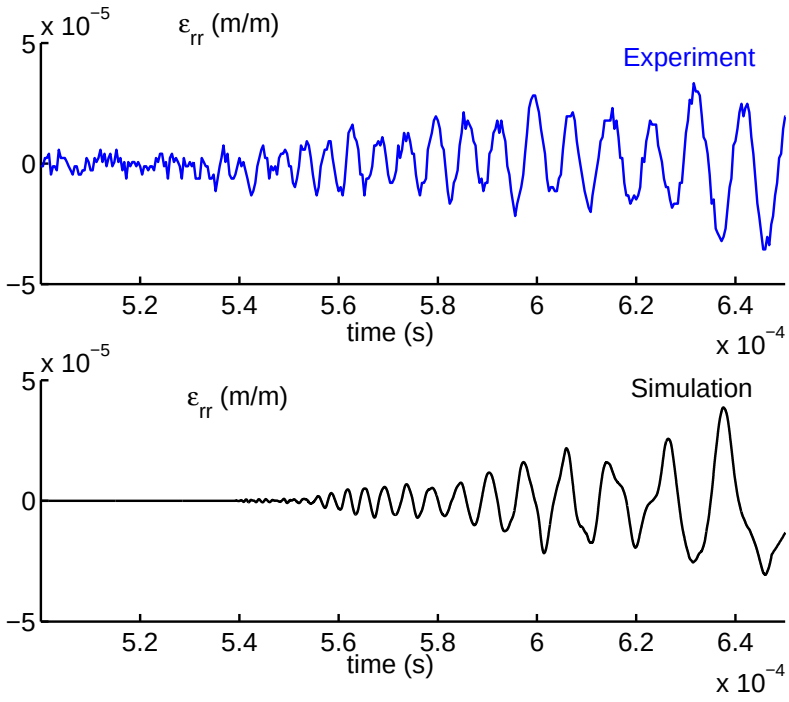

Figure 17: Simulation and experimental results for configuration 2, 62.5-283, at $r = 300$ mm.

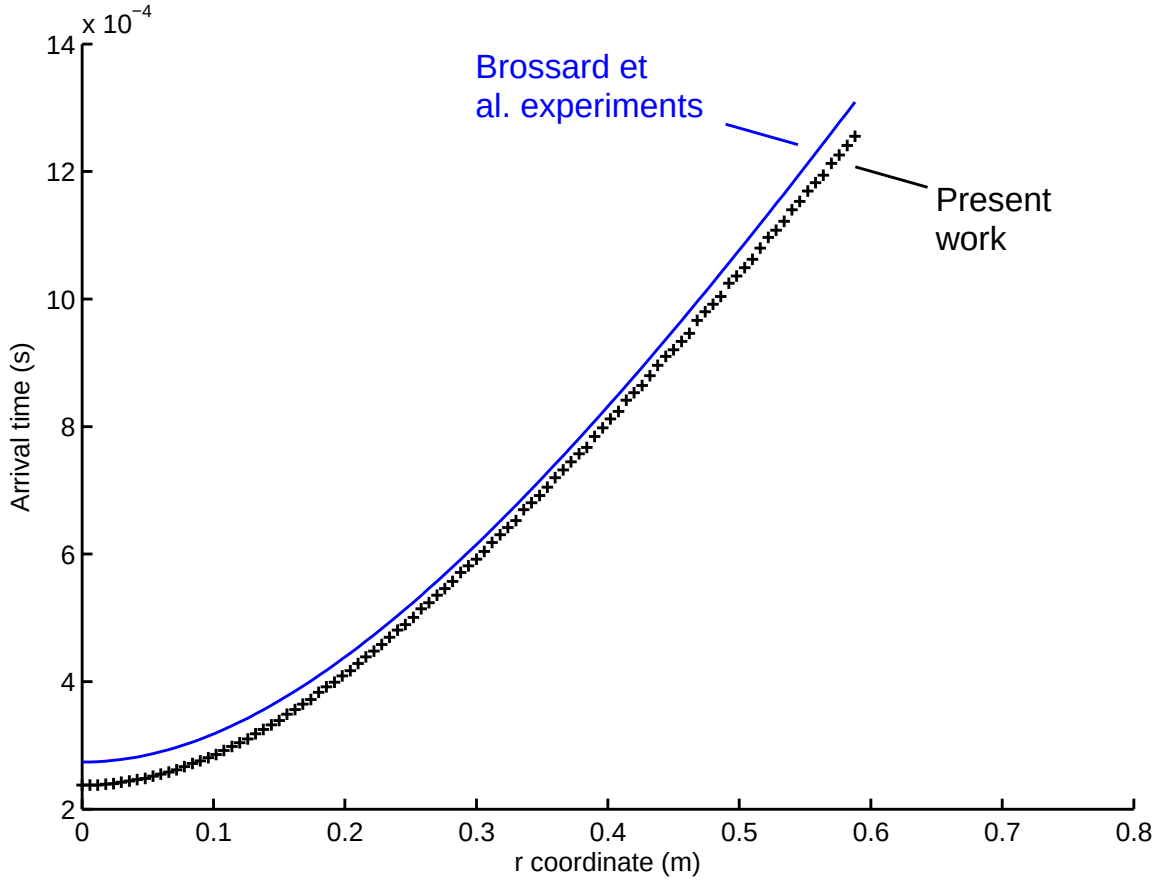

Figure 18: Arrival time vs. r coordinate.

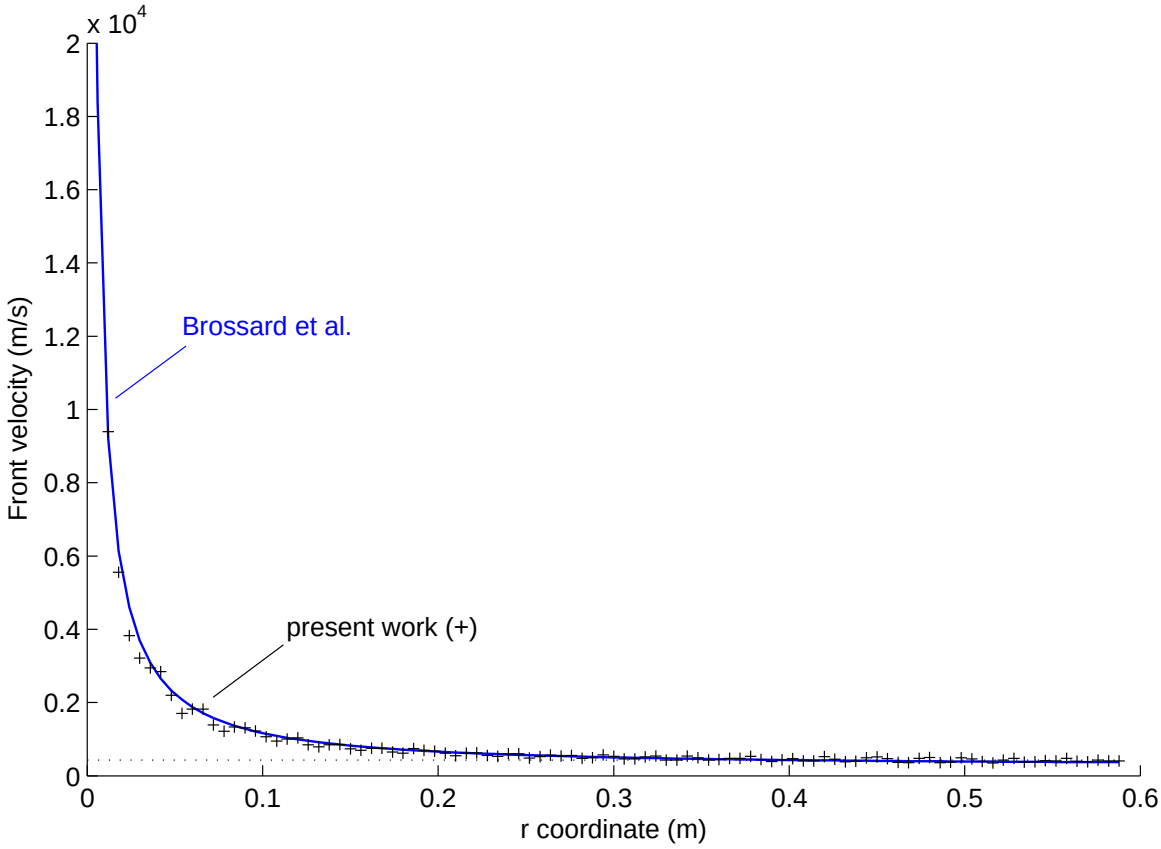

Figure 19: Front velcocity vs. r coordinate.